Advanced Ceramics Progress: Vol. 7, No. 4, (Autumn 2021) 20-27

Materials and Energy Research Center
MERC

Contents lists available at ACERP

Advanced Ceramics Progress

Journal Homepage: www.acerp.ir

Original Research Article

Multi-Walled Carbon Nanotubes (MWCNTs) Synthesized on Ni-Cu NPs @ a-C: H Films: A Study of Cavity and Bearing Areas Percentage, ZX Topography, and the Width of the Surface Height Distribution with Different Ni Layers' Thickness

V. Dalouji [a,*], S. Goudarzi [b], N. Rahimi [b], A. R. Souri [c]

[a] *Associate Professor, Department of Physics, Faculty of Science, Malayer University, Malayer, Hamadan, Iran*
[b] *PhD Student, Department of Physics, Faculty of Science, Malayer University, Malayer, Hamadan, Iran*
[c] *Assistant Professor, Department of Materials Engineering, Faculty of Engineering, Malayer University, Malayer, Hamadan, Iran*

* Corresponding Author Email: dalouji@yahoo.com (V. Dolouji)

URL: https://www.acerp.ir/article_144166.html

ARTICLE INFO

Article History:

Received 13 December 2021
Received in revised form 15 January 2022
Accepted 01 February 2022

Keywords:

Topography
Bearing Area
Nanotubes Lateral Size
Fractal Dimensions
Optical Density

ABSTRACT

Topological characterizations and optical density of the synthesized hydrogenated amorphous carbon Cu-Ni NPs @ a-C: H nanotubes (CNTs) with different surface morphology were studied in this report. Films deposited with Ni layer thickness of 5 nm have a maximum value of optical density especially, in the high energy range. Steps between 1800 to 2000 KeV in the Rutherford backscattering (RBS) spectra correspond to the presence of Cu and Ni elements. The thicknesses of films were measured by using SIMN-RA software. Films deposited with Ni layer thickness of 15 nm have a maximum value of the lateral size of nanotubes in about 19.7 nm. The grown CNTs of films deposited with Ni layer thickness 15 nm Ni, has a maximum value of diameter in about 16.2 nm. The diagram of bearing area proportion height shows the percentage of cavities and single-layers. The cavity coverage of films was less than 5 % and the layer content of films was about 90 %.

https://doi.org/10.30501/ACP.2022.318678.1077

1. INTRODUCTION

The study of physical properties of metallic nanoparticles in dielectric host medium has been the subject of extensive research due to their unique applications in many areas such as nonlinear optical switching, immunoassay labeling, and Raman spectroscopy enhancement [1,2]. Especially copper-nickel nanoparticles have received significant attention due to their potential applications in optical magnetic recording, spintronics, data storage devices, and used as giant magnetic resistance (GMR) [3]. Cu-Ni nanoparticles have been also used as catalysts for the synthesis of dimethyl carbonate and carbon nanotubes [4-6]. Multilayers with a thickness of two layers less than 100 nm that are inaccessible in bulk have very

Please cite this article as: Dalouji, V., Goudarzi, S., Rahimi, N., Souri, A. R., "Multi-Walled Carbon Nanotubes (MWCNTs) Synthesized on Ni-Cu NPs @ a-C: H Films: A Study of Cavity and Bearing Areas Percentage, ZX Topography, and the Width of the Surface Height Distribution with Different Ni Layers' Thickness", ***Advanced Ceramics Progress***, Vol. 7, No. 4, (2021), 20-26. https://doi.org/10.30501/ACP.2022.318678.1077

interesting properties due to their magnetic properties and improvement of their mechanical properties [7]. Although the study of the surface structure and interface at the atomic scale of such layers is a very difficult task in surface science the results which are obtained from these studies are very important. Plasma arc evaporation [8] and sol-gel methods [9] were used to make copper-nickel alloy nanoparticles. Amorphous carbon metals have many applications as coatings in optical, electronic, mechanical, and biomedical applications [6-9]. Since the discovery of carbon nanotubes, there has been a great deal of interest in synthesizing the growth of directed nanotubes [10]. The reason for the interest in nanotubes is due to their excellent physical properties such as high mechanical strength, high dimensional ratio, and good thermal conductivity [11,12]. In recent years, there have been extensive publications to prove the growth of both random and homogeneous nanotubes [13-16]. However, for applications where nanotubes act as electrical conductors, the growth of directional carbon nanotubes is preferred. Normally, nanotubes grow in a manner such as chemical vapor deposition (CVD) on metal catalyst particles or islands located on top of a semiconductor or insulating substrate. However, for many of the predicted programs, it is best to grow the nanotubes directly on a conventional copper-like substrate to provide good power. Since copper itself is not a suitable catalyst for the growth of carbon nanotubes, the technique discussed here uses nickel-transfer metal as a catalyst in copper substrates. Esconjauregu et al. have reported that among metals Ni, Fe, Co, and their alloys act as the best catalyst for direct growth of carbon nanotubes [17-19]. Nickel was selected as a catalyst due to its superior properties for achieving directional carbon nanotube growth [20-23]. CNT growth is difficult on bulk copper unless it is in the form of nanoparticles or several layers of metal catalysts are stored in it. In this work, the effect of different Ni layers' thickness was studied on optical density, surface topography, and the fractal dimensions of films.

2. EXPERIMENTAL DETAILS

More details of the sputtering deposition process were given in references [3-5]. The scheme of co-deposition by RF-Sputtering and RPECVD techniques is shown in Figure 1. Cu-Ni NPs @ a-C: H with different thicknesses of Ni overlayer is provided by a capacitance coupled radio frequency plasma enhanced chemical vapor deposition (RF-PECVD) system with a 13.56 MHz power supply. The reactor is composed of two electrodes with different area sizes. The electrode smaller was Cu and Ni targets at the first and the second stages of deposition. Another electrode was placed in the body of the stainless-steel chamber. All deposition was performed at room temperature on this electrode over the glass and silicon substrates. The chamber was vacuumed to a base pressure of 10^{-5} mbar before to the deposition then the pressure was increased to ambient pressure by acetylene gas. The RF power 200 W and initial gas pressure were at different pressures from 0.01 mbar to 0.05 mbar. The copper deposition time was 20 minutes. After the deposition of copper, the electrode was changed to Ni, and sputtering was done for 2 min with RF power of 250 W and acetylene initial pressure of 0.025 mbar. To obtain chemical compounds and the thickness of the prepared thin films, the RBS spectra were obtained using a helium ion beam with energy of about 2 MeV. The thickness of the films and the atomic content of the films were obtained from RBS data by SIMN-RA software simulation and the thicknesses of films were kept constant and were measured from RBS spectra. In order to study the surface topography of the thin films and the average nanotube's size atomic force microscopy *(*AFM*)* analysis in the noncontact mode was used. By using of a double beam UV-Vis spectrometer, the optical densities of films were measured. The Thermal Chemical Vapor Deposition (TCVD) system includes a furnace, a quartz tube of 60 cm length and 40 mm inner diameter, a temperature controller with a thermocouple. The LP gas (LPG) with a flow of 80 sccm and at 825 °C was applied to the reactor. The composition of PLG was measured by a gas chromatograph (Hewlett Packard, Palo Alto, CA, USA) and it was a mixture of C3 (54 %), C4 (45 %), and C5 (1 %).

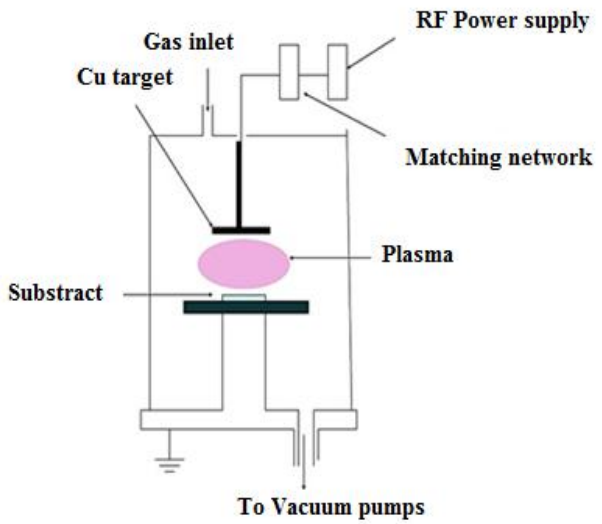

Figure 1. (Color online) The scheme of co-deposition by RF-Sputtering and RPECVD setup [4]

3. RESULTS AND DISCUSSION

To obtain the optical density of films Equation (1) was used [24,25]:

$$D_{opt} = 2.303\ A \quad (1)$$

Here A is the absorbance of the films. Figure 2 shows the optical density of the films with various thicknesses of Ni layers. As it is clear the optical density for films is constant between 1 and 3 eV, and then increases with a relatively slow slope. The optical density of films containing Ni with a thickness of about 5 nm has a maximum value. However, the sizes of nanotubes show very significant changes with photon energy for Ni films with a layer thickness of 15 nm [26].

From RBS spectra (It has been reported in previous works [27]) it is possible to find out Cu, Ni, C , and O contents of the samples. In RBS spectra, steps at 1550 and 1700 KeV could be respectively due to O and Si nuclei of the amorphous SiO_2 substrate. Peaks at 1400 KeV and in the range 1800 to 1900 KeV were attributed to C, Cu , and Ni nuclei, respectively. The peak between 1800 and 1900 KeV is considered a convoluted peak. Their results of SIMN-RA software simulation of RBS spectra indicate that the Cu layer contains 40 % Cu, 55 % C, and 5 % O , and its thickness is about 100 nm. This is common among all prepared samples. The composition of Ni layers was obtained 80 % Ni, 10 % C, and 10 % O , and the thicknesses of these over layers for the samples with 2.7- and 10-min deposition were obtained 5, 10, and 15 nm, respectively. It is clearly observable that the intensity of RBS spectra was increased by the increase of the thickness of Ni layers.

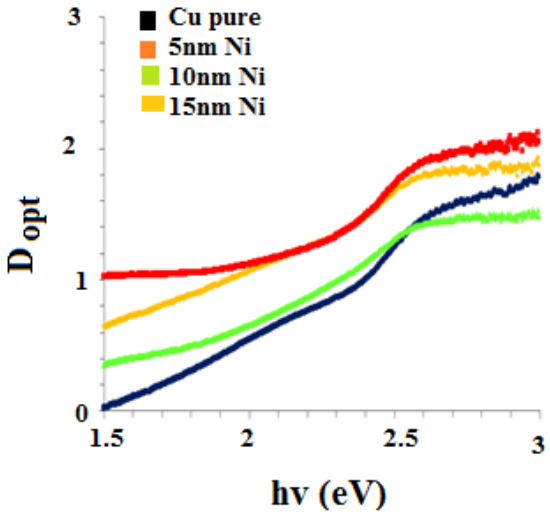

Figure 2. Optical density of films for Cu pure, Ni layer thickness 5 nm, 10 nm, and 15 nm

The SEM images of films with and without Ni for layers with 5, 10, and 15 nm thicknesses are shown in Figure 3(a-d), respectively. As it is clear by adding Ni the density of the CNTs is greatly enhanced. Furthermore, the average diameter of the grown CNTs depends on the Ni content and increases by increasing Ni content. The average diameter of the grown CNTs on films for Ni layers of thickness 5, 10, and 15 nm Ni are obtained about 10.3, 12.5, and 16.2 nm, respectively. As it is clear from Fig. 3(d) which shows the SEM image of films with 15 nm thickness, MWCNTs are formed on the films, shorter nanotubes are formed and the quality and height of these nanotubes in the third sample are higher than the other samples.

The surface morphology and the average nanoparticle size of films were obtained by AFM in non-contact mode and the results are shown in Figure 4. The nanotubes lateral size of the thin films can be estimated using AFM images. The variations of nanotubes lateral sizes of films surfaces versus different the Ni layer

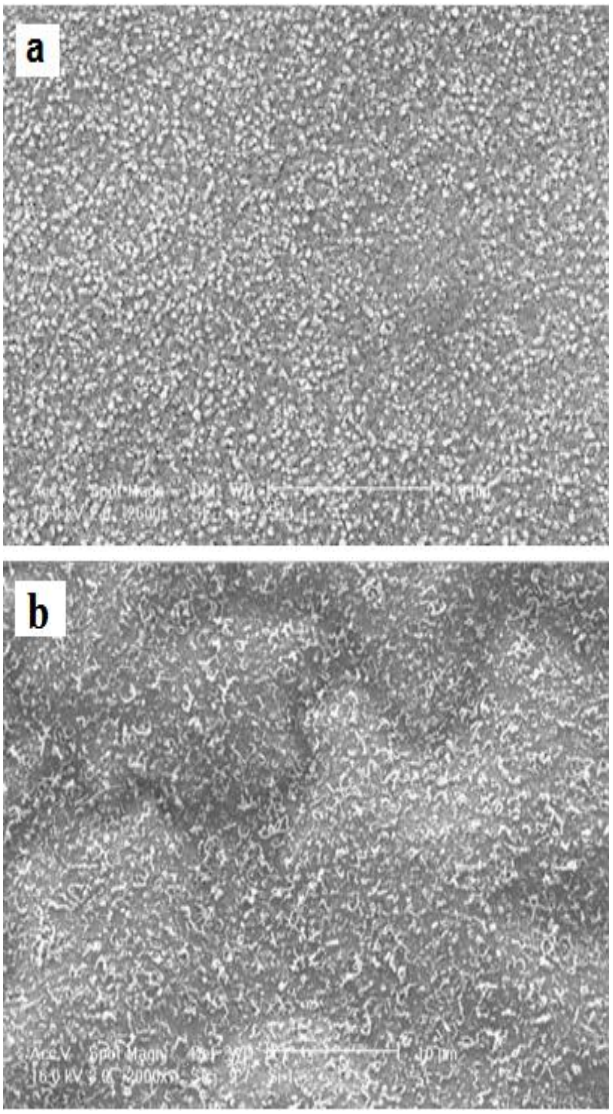

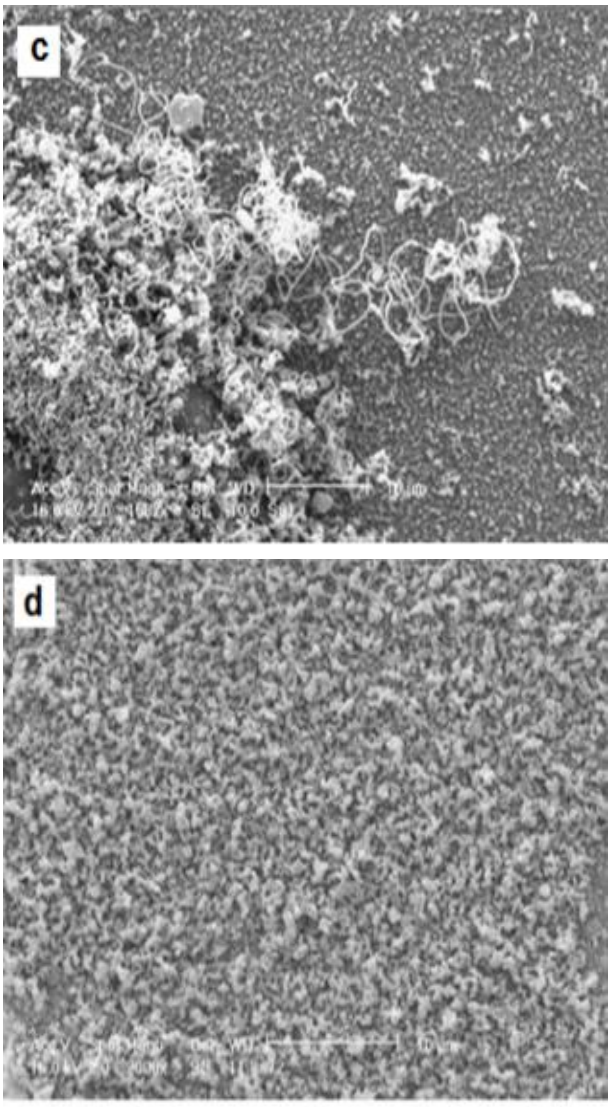

Figure 3. SEM images of films for different Ni layer thickness (a) Cu pure, (b) Ni-5 nm, (c) Ni-10 nm, and (d) Ni-15 nm

thicknesses for different deposited films, Cu pure layer, Ni-5 nm, Ni-10 nm, and Ni-15 nm were about 12, 14.4, 13.2, and 19.7 nm for films, respectively (Figure 5). The films deposited with a layer of Ni with a thickness of 15 nm have maximum nanotubes lateral size, however, Cu pure layer has a minimum of nanotubes lateral size. The AFM images show that the nanotubes synthesized on the substrates, firstly, have a uniform distribution that is distributed throughout the substrates, and secondly, at the measuring scale, the mean diameter values of the measured nanotubes also appear to be almost identical. It was found that the size of nanotubes on films surfaces was increased with the increasing of the Ni thickness of the Ni layer from 5 nm, then it was decreased up to 10 nm and from 10 to 15 nm it was increased. The nanotube's size changes as Gaussian plots, which can almost be due to little changes in the size of the nanotubes with the change in thickness of the Ni layers. The AFM images for similar substrates were reported earlier [28]. By comparing SEM and AFM images we find that both are compatible with each other. It can be seen that in the pictures, CNTs have different diameters and in general the average diameter of grown carbon nanotubes increases with increasing thickness of nickel layers.

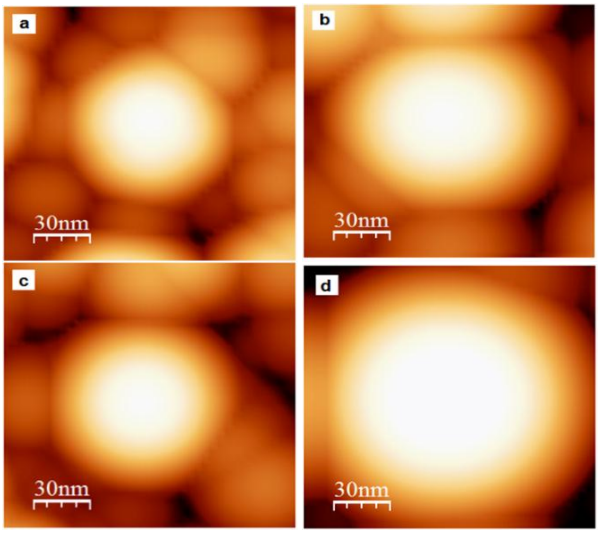

Figure 4. AFM images of films for different Ni layer thickness (a) Cu pure, (b) Ni-5 nm, (c) Ni-10 nm, and (d) Ni-15 nm

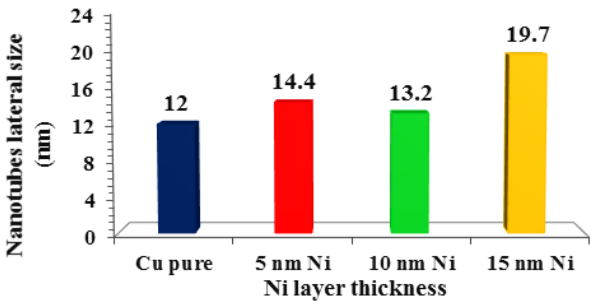

Figure 5. The variations of nanotubes lateral size of nanoparticles on the surface of films for Cu pure, Ni-5 nm, Ni-10 nm, and Ni-15 nm

Figure 6 (a-d) shows the variations in the height of the thin films on the surface versus the x and z axes for films without Ni thin layer and with layer contenting Ni layer of thicknesses 5, 10, and 15 nm, respectively. The scanning size on the surface of the films for the AFM study was chosen as much as 1 μm × 1 μm (the maximum scale value on the x-axis was as much as 1 μm). The height's changes on the surface of the scanned films show that the films have a topological phase-change films. In the deposited films, the *z* values

were about 13 nm for the thin layer contenting Ni thickness layer 5 nm, Ni thickness layer 10 nm, Cu pure, and about 17 nm for Ni thickness layer 15 nm. These results show that the films are smooth in this state and showed a second phase change. The films without Ni thin films have lower fluctuations, and the peaks have a slower slope than other thin layers contenting Ni thickness layer. The *z* variations versus *x* variations are closely related to both Cu and Ni materials, which have many peaks.

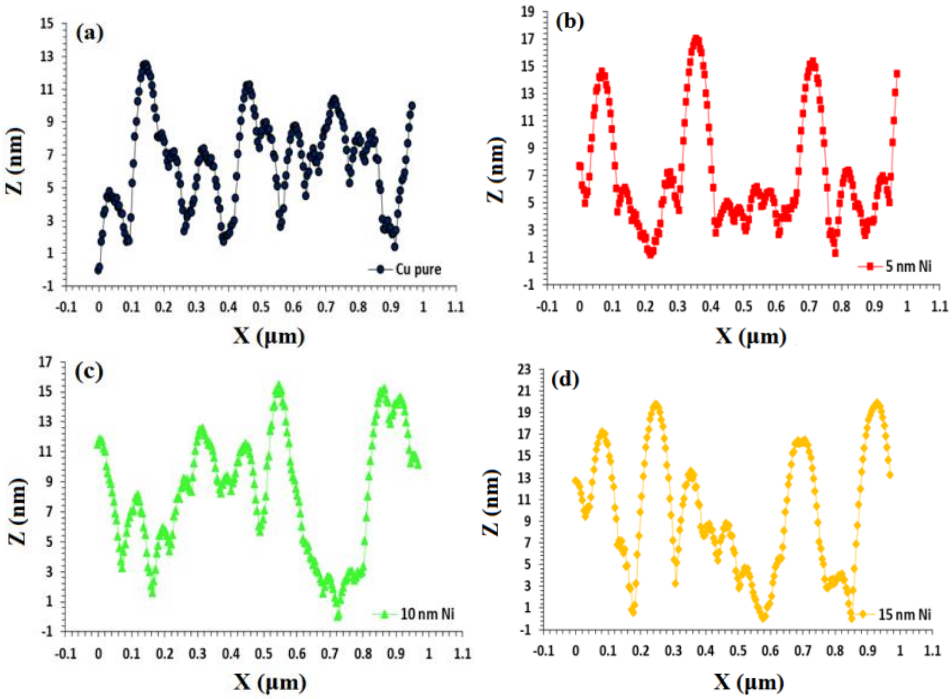

Figure 6. Z-height variations of nanoparticles on the surface of films versus x-axis of the films for different Ni thickness layer (a) Cu pure (b) Ni-5 nm, (c) Ni-10 nm, and (d) Ni-15 nm

The PSD spectra were extracted from the scanned area and 30 nm obtained from AFM images of the films as shown in Figure 4. It can be seen that all the PSD points include a high spatial frequency region. According to the Dynamic Scaling Theory (DST), the power spectral densities (PSDs) analyses closely show how the roughness varies with length scale. The AFM images can be divided into pixels as a small square area where the vectors h(xi) and h(yj) are the height at (xi, yj) positions. Then, the one-dimensional average of the power spectral densities (PSDs) is given as follows:

$$P(k) \propto \frac{2L}{N}\left[\langle\sum_{i=1}^{\frac{N}{2}}\left(FFT\left(h(x_i)\right)^2\right)\rangle_y + \langle\sum_{i=1}^{\frac{N}{2}}\left(FFT\left(h(y_i)\right)^2\right)\rangle_x\right] \quad (2)$$

Where FFT is the Fast Fourier Transform between the real and reciprocal spaces.

According to the dynamical scaling theory, the relation P (k) and frequency k are given below for a system with lateral size L [29]:

$$P(k) \propto k^{-\beta} \quad (3)$$

Here β is calculated from the slope of the log-log in PSD spectra of high spatial frequency. The fractal dimensions D_f of films are obtained by solving the β slope of the log-log graph [28]:

$$D_f = 4+\beta/2 \quad (4)$$

Figsure 7 (a-d) show the variations of spectral density with a spatial frequency of films for: (a) pure Cu and Ni layers with thicknesses (b) 5 nm, (c) 10 nm, and (d) 15 nm. Especially in the high spatial frequency region, the spectral compaction power of all films reflects the inverse current power variations and indicates the attendance of fractal components in outstanding topographies. From these values, one can determine the relative amounts of surface disorder at various distance scales. As the thicknesses of Ni layers were increased, the performance of the spectral compaction power increases as a result of decreasing the size of the nanotubes. The Ni layer with 15 nm thickness and the pure Cu layers have maximum and minimum values of the fractal dimensions, respectively.

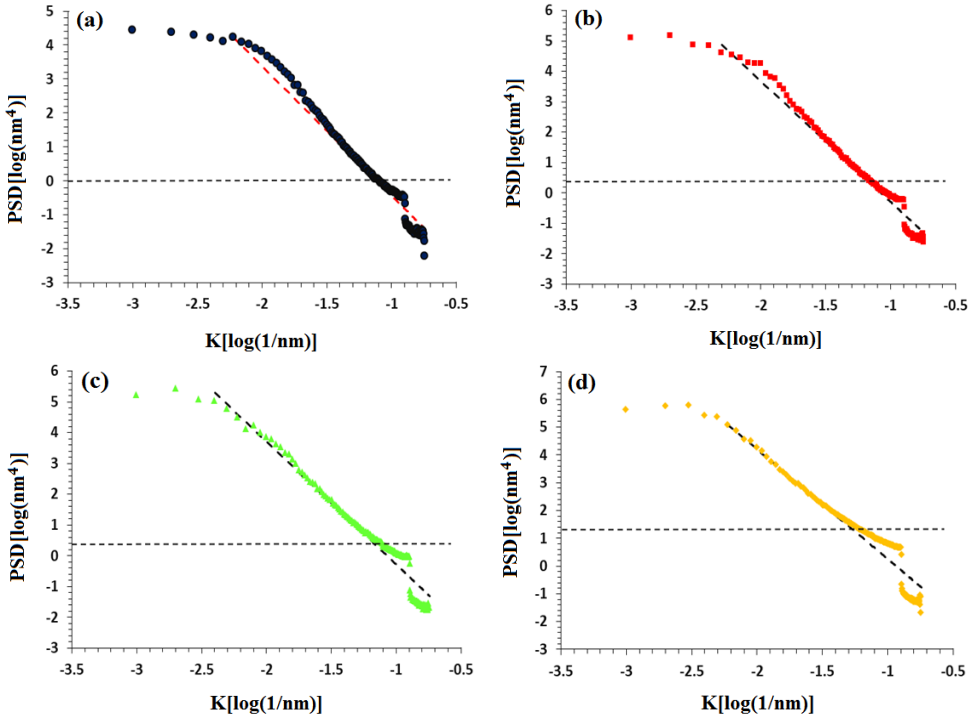

Figure 7. The variations of power spectral density of the films versus frequency k of films for different Ni layer thickness(a) Cu pure, (b) Ni-5 nm, (c) Ni-10 nm, and (d) Ni-15 nm

Figure 8 shows illustrate the variations of fractal dimensions versus of Ni layer thickness. The fractal dimensions of films for pure Cu films and Ni layers with thicknesses 5, 10, and 15 nm were estimated to be 2.92, 2.98, 2.95, and 2.93 nm, respectively. Therefore, the fractal dimensions of films increase with the increase of the Ni thickness layer up to 5 nm, and then, it was decreased over 5 nm.

Figure 9 shows the variations of bearing area of the films in respect to Ni layer thickness for Ni layers of thickness 5 nm, 10 nm, and 15 nm. The area shows the tolerance for height. In fact, it indicates the amount of vacuum, zero coverage (cavity, bottom curvature of the diagram), monolayer (upper curvature of the diagram), and isolation (between the cavity and monolayer) of the layers. The films in Cu pure, Ni thickness layer 5 nm, Ni thickness layer 10 nm have cavity coverage of less than 5 % and layer content of about 90 % and 95 % which are monolayer height. In the vacuum, Ni thickness layer is 15 nm, the coating is 10 %, and the content of the film is about 90 %, 80 % of which is isolated. Thickness did not have much effect on the degree of isolation, so all four diagrams have similar results.

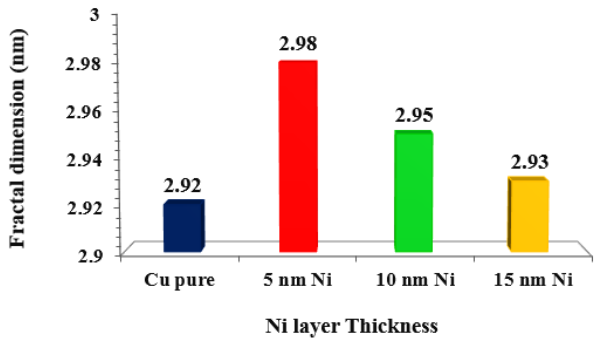

Figure 8. The variations of fractal dimensions of films for Cu pure, Ni-5 nm, Ni-10 nm, and Ni-15 nm

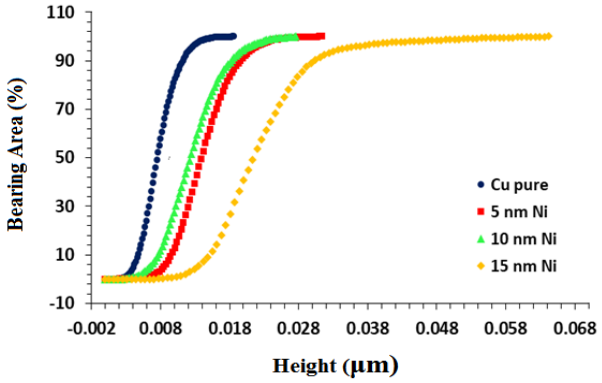

Figure 9. The bearing areas of films for Cu pure, Ni-5 nm, Ni-10 nm, and Ni-15 nm

4. CONCLUSION

In this article, we show that films have an important effect on the growth of MWCNTs based on Ni NPs catalyst. The optical density of films with a layer of Ni and thickness of 5 nm has the maximum value. The optical density and the average diameters of the grown CNTs increase with increasing Ni layer thickness. The average diameter of CNTs of films with a 15 nm layer of Ni is 17 nm. The AFM images show that the nanotubes synthesized on the substrates both have a uniform distribution and the mean diameter values of the measured nanotubes also appear to be almost identical. We found that the fractal dimensions of films were decreased with the increase of the thickness of the Ni layer. Thickness did not have much effect on the degree of isolation, so all four diagrams have similar results.

ACKNOWLEDGEMENTS

The authors would like to acknowledge the financial support of Malayer University for this research.

REFERENCES

1. Li, X., Lv, M., Tian, Y., Gao, L., Liu, T., Zhou, Q., Xu, Y., Shen, L., Shi, W., Li, X., Lu, Y., "Negatively charged polymeric interphase for regulated uniform lithium-ion transport in stable lithium metal batteries", ***Nano Energy***, Vol. 87, (2021), 106214. https://doi.org/10.1016/j.nanoen.2021.106214
2. Genov, D. A., Seal, K., Sarychev, A. K., Noh, H., Shalaev, V. M., Ying, Z. C., Zhang, X., Cao, H., "Surface plasmon delocalization by short-range correlations in percolating metal systems", ***Applied Physics B***, Vol. 84, No. 1, (2006), 205-210. http://doi.org/10.1007/s00340-006-2229-7
3. Singh, S., Basu, S., Ghosh, S. K., "Structure and morphology of Cu/Ni film grown by electrodeposition method: A study of neutron reflectivity and AFM", ***Applied Surface Science***, Vol. 255, No. 11, (2009), 5910-5916. https://doi.org/10.1016/j.apsusc.2009.01.030
4. Zhou, Y., Wang, S., Xiao, M., Han, D., Lu, Y., Meng, Y., "Formation of dimethyl carbonate on nature clay supported bimetallic copper-nickel catalysts", ***Journal of Cleaner Production***, Vol. 103, (2015), 925-933. https://doi.org/10.1016/j.jclepro.2014.08.075
5. Bian, J., Xiao, M., Wang, S. J., Lu, Y. X., Meng, Y. Z., "Graphite oxide as a novel host material of catalytically active Cu–Ni bimetallic nanoparticles", ***Catalysis Communications***, Vol. 10, No. 11, (2009), 1529-1533. https://doi.org/10.1016/j.catcom.2009.04.009
6. Zhang, M., Yang, K., Zhang, X., Yu, Y., "Effect of Ni (111) surface alloying by Pt on partial oxidation of methane to syngas: A DFT study", ***Surface Science***, Vol. 630, (2014), 236-243. https://doi.org/10.1016/j.susc.2014.08.023
7. Tokarz, A., Fraczek, T., Balaga, Z., Nitkiewicz, Z., "Structure, hardness and thermal stability of electrodeposited Cu/Ni nanostructured multilayers", ***Reviews on Advanced Materials Science***, Vol. 15, No. 3, (2007), 247-252. https://www.ipme.ru/e-journals/RAMS/no_31507/tokarz.pdf
8. Liu, H. D., Yang, B., Mao, M. R., Liu, Y., Chen, Y. M., Cai, Y., Fu, D. J., Ren, F., Wan, Q., Hu, X. J., "Enhanced thermal stability of solar selective absorber based on nano-multilayered TiAlON films deposited by cathodic arc evaporation", ***Applied Surface Science***, Vol. 501, (2020), 144025. https://doi.org/10.1016/j.apsusc.2019.144025
9. Phin, H. Y., Ong, Y. T., Sin, J. C., "Effect of carbon nanotubes loading on the photocatalytic activity of zinc oxide/carbon nanotubes photocatalyst synthesized via a modified sol-gel method", ***Journal of Environmental Chemical Engineering***, Vol. 8, No. 3, (2020), 103222. https://doi.org/10.1016/j.jece.2019.103222
10. Ajayan, P. M., Ebbesen, T. W., Ichihashi, T., Iijima, S., Tanigaki, K., Hiura, H., "Opening carbon nanotubes with oxygen and implications for filling", ***Nature***, Vol. 362, No. 6420, (1993), 522-525. https://doi.org/10.1038/362522a0
11. Harris, P. J. Hernández, E., Yakobson, B. I., "Carbon Nanotubes and Related Structures: New Materials for the Twenty-First Century", ***American Journal of Physics***, Vol. 72, No. 3, (2004), 415-415. https://doi.org/10.1119/1.1645289
12. Dresselhaus, M. S., Dresselhaus, G., Eklund, P. C., ***Science of Fullerenes and Carbon Nanotubes: Their Properties and Applications***, Elsevier, (1996). https://doi.org/10.1016/B978-0-12-221820-0.X5000-X
13. Ebbesen, T. W., Ajayan, P. M., Hiura, H., Tanigaki, K., "Purification of nanotubes", ***Nature***, Vol. 367, No. 6463, (1994), 519-519. https://doi.org/10.1038/367519a0
14. Ren, Z., Lan, Y., Wang, Y., "Technologies to Achieve Carbon Nanotube Alignment", In ***Aligned Carbon Nanotubes***, Springer, Berlin, Heidelberg, (2012), 111-156. https://doi.org/10.1007/978-3-642-30490-3_6
15. Dhore, V. G., Rathod, W. S., Patil, K. N., "Synthesis and characterization of high yield multiwalled carbon nanotubes by ternary catalyst", ***Materials Today: Proceedings***, Vol. 5, No. 2, (2018), 3432-3437. https://doi.org/10.1016/j.matpr.2017.11.589
16. Li, M., Liu, X., Zhao, X., Yang, F., Wang, X., Li, Y., "Metallic catalysts for structure-controlled growth of single-walled carbon nanotubes", ***Single-Walled Carbon Nanotubes***, (2019), 25-67. https://doi.org/10.1007/s41061-017-0116-9
17. Esconjauregui, S., Whelan, C. M., Maex, K., "The reasons why metals catalyze the nucleation and growth of carbon nanotubes and other carbon nanomorphologies", ***Carbon***, Vol. 47, No. 3, (2009), 659-669. https://doi.org/10.1016/j.carbon.2008.10.047
18. Li, Y. S., Hirose, A., "Controlled synthesis of diamond and carbon nanotubes on Ni-base alloy", ***Applied Surface Science***, Vol. 255, No. 5, (2008), 2251-2255. https://doi.org/10.1016/j.apsusc.2008.07.076
19. Gao, L., Peng, A., Wang, Z. Y., Zhang, H., Shi, Z., Gu, Z., Cao, G., Ding, B., "Growth of aligned carbon nanotube arrays on metallic substrate and its application to supercapacitors", ***Solid State Communications***, Vol. 146, No. 9-10, (2008), 380-383. https://doi.org/10.1016/j.ssc.2008.03.034
20. Bonnet, F., Ropital, F., Berthier, Y., Marcus, P., "Filamentous carbon formation caused by catalytic metal particles from iron oxide", ***Materials and Corrosion***, Vol. 54, No. 11, (2003), 870-880. https://doi.org/10.1002/maco.200303742
21. Guevara, L., Wanner, C., Welsh, R., Atwater, M. A., "Using mechanical alloying to create bimetallic catalysts for vapor-phase carbon nanofiber synthesis", ***Fibers***, Vol. 3, No. 4, (2015), 394-410. https://doi.org/10.3390/fib3040394
22. Kharlamova, M. V., "Investigation of growth dynamics of carbon nanotubes", ***Beilstein Journal of Nanotechnology***, Vol. 8, No. 1, (2017), 826-856. https://doi.org/10.3762/bjnano.8.85
23. Kharlamova, M. V., Eder, D., "Carbon nanotubes: Synthesis, properties, and new developments in research", ***Synthesis and Applications of Nanocarbons***, (2020), 107-147. https://doi.org/10.1002/9781119429418.ch4
24. Hassanien, A. S., Akl, A. A., "Effect of Se addition on optical and electrical properties of chalcogenide CdSSe thin films", ***Superlattices and Microstructures***, Vol. 89, (2016), 153-169. https://doi.org/10.1016/j.spmi.2015.10.044
25. Dalouji, V., Goudarzi, S., Solaymani, S., "The optical density and topography characterizations of MWCNTs on Ni-Cu/a-C: H

substrates with different copper percentage", ***Microscopy Research and Technique***, Vol. 84, No. 6, (2021), 1205-1211. https://doi.org/10.1002/jemt.23679

26. Dejam, L., Solaymani, S., Achour, A., Stach, S., Ţălu, Ş., Nezafat, N. B., Dalouji, V., Shokri, A. A., Ghaderi, A., "Correlation between surface topography, optical band gaps and crystalline properties of engineered AZO and CAZO thin films", ***Chemical Physics Letters***, Vol. 719, (2019), 78-90. https://doi.org/10.1016/j.cplett.2019.01.042
27. Dalouji, V., Rahimi, N., Goudarzi, S., Solaymani, S., "MWCNTs synthesized on Ni Cu NPs @ aC: H films: study of the dielectric relaxation time, the free carriers concentration and the dissipation factor with different Ni layers thickness", ***Optical and Quantum Electronics***, Vol. 53, No. 11, 648, (2021), 1-13. https://doi.org/10.1007/s11082-021-03289-w
28. Hedayati, K., "Structural and magnetic characterization of electrodeposited Ni–Cu/Cu and Fe–Ni–Cu/Cu multilayer", ***Applied Physics A***, Vol. 118, No. 3, (2015), 975-979. https://doi.org/10.1007/s00339-014-8851-z
29. Rahimi, N., Dalouji, V., Souri, A., "Studying the optical density, topography, and structural properties of CZO and CAZO thin films at different annealing temperatures", ***Advanced Ceramics Progress***, Vol. 6, No. 2, (2020), 17-23. https://doi.org/10.30501/acp.2020.107466